Geometric Accuracy Assessment of QuickBird Basic Imagery Using Different Operational Approaches

Manuel A. Aguilar, Fernando J. Aguilar, Francisco Agüera, and Jaime A. Sánchez

Abstract

The new very high-resolution space satellite images, such as QuickBird and Ikonos, open new possibilities in cartographic applications. This work has as its main aim the assessment of a methodology to achieve the best possible geometric accuracy in orthorectified imagery products obtained from QuickBird basic imagery which will include an assessment of the methodology's reliability. Root Mean Square Error (RMSE), mean error or bias, and maximum error in 79 independent check points are computed and utilized as accuracy indicators.

The ancillary data were generated by high accuracy methods: (a) check and control points were measured with a differential global positioning system, and (b) a dense digital elevation model (DEM) with grid spacing of 2 m and $RMSE_z$ of about 0.31 m generated from a photogrammetric aerial flight at an approximate scale of 1:5000 that was used for image orthorectification. Two other DEMs with a grid spacing of 5 m ($RMSE_z$ = 1.75 m) and 20 m ($RMSE_z$ = 5.82 m) were also used.

Four 3D geometric correction models were used to correct the satellite data: two terrain-independent rational function models refined by the user, a terrain-dependent model, and a rigorous physical model. The number and distribution of the ground control points (GCPs) used for the sensor orientation were studied as well, testing from 9 to 45 GCPs. The best results obtained about the geometric accuracy of the orthorectified images (two dimensional RMSE of about 0.74 m) were computed when the dense DEM was used with the 3D physical and terrain-dependent models. The use of more than 18 GCPs does not improve the results when those GCPs are extracted by stratified random sampling.

Introduction

Since the successful launch in the recent past of very high-resolution sensors, especially Ikonos with 1 m Ground Sample Distance (GSD) and QuickBird with 0.61 GSD, many researchers have considered them as possible substitutes of the classical aerial images used for large scales cartographic purposes (Fraser, 2002; Kay *et al.*, 2003; Chmiel *et al.*, 2004; Pecci *et al.*, 2004). Besides, in the near future, several high-resolution optical space systems will be put in operation, resulting in improvements in the resolution, availability, and cost.

Nowadays, the cost of acquiring such mapping products (e.g., Ikonos Pro or QuickBird Orthorectified Imagery) is quite considerable, however, there are methods available for users with photogrammetric capability to generate high accuracy mapping at the lowest cost from basic products such Ikonos Geo or QuickBird Basic Imagery.

To obtain orthorectified images of very high-resolution imagery, regardless of the raw data format, it is necessary to have into account the following steps: (a) acquisition of image(s) and metadata, (b) acquisition of the coordinates *X, Y, Z* of ground points, ground control points (GCPs) and independent check points (ICPs), (c) to obtain the image coordinates of these points, (d) computation of the unknown parameters of the 3D geometric correction model used, and finally (e) image(s) orthorectification using a digital elevation model (DEM).

The resulting orthoimage can then be directly applied in Geographic Information Systems (GIS) or mapping oriented area applications. In fact, in European Union countries, the agricultural policies are culminating in the official requeriment for the obligatory use of GIS techniques to control the subsidy payments. These Agri-GIS systems require very accurate orthoimages, and they can be obtained from very high-resolution satellite data (Rossi and Volpe, 2005).

When high accuracy is required in the orthorectification process, the ancillary data (GCPs, DEM) must be of high quality (Lingua and Borgogno, 2003; Chmiel *et al.*, 2004; Toutin and Chénier, 2004). With GCPs measured by differential global positioning system (DGPS), the predominant error comes from image pointing. Therefore, the selection of points that are very well-defined in the image is very important. A good distribution of GCPs can improve accuracy (Zhou and Li, 2000), and it should be spread over the whole image such in planimetry as in the elevation range (Toutin, 2004a).

The main aim of this paper is the study of different methodological approaches to achieve the best possible geometric accuracy in orthorectified imagery products obtained from panchromatic QuickBird basic imagery in an operational environment. At the same time the study will also focus on the reliability of the operational approaches. The following variation sources have been studied:

Department of Agricultural Engineering, Almería University, Ctra. de Sacramento s/n, La Cañada de San Urbano, Escuela Politécnica Superior, 04120, Almería, Spain (maguilar@ual.es).

Photogrammetric Engineering & Remote Sensing
Vol. 73, No. 12, December 2007, pp. 1321–1332.

0099-1112/07/7312–1321/$3.00/0

1. Four sensor orientation or 3D geometric correction models have been used to correct the satellite data.
2. Number of GCPs used to compute the 3D geometric correction models (9, 18, 27, 36, and 45).
3. Random and stratified random samplings for the combinations of 9 and 18 GCPs.
4. Accuracy of the DEM employed in imagery orthorectification.

Image Correction Models

In satellite imagery, a sensor model or geometric correction model relates object point positions (*X, Y, Z*) to their corresponding 2D image positions (*x, y*). It is solved in aerial photogrammetry by means of the known colinearity equation (e.g., Wong, 1980). Several sensor models can be used to correct satellite imagery: 2D polynomial functions, 3D polynomial functions, affine model, 3D rational functions, and 3D physical models (Tao and Hu, 2001; Jacobsen, 2002; Fraser *et al.*, 2002; Fraser and Yamakawa, 2004; Toutin, 2004a).

However, for the 3D geometric correction of very high-resolution satellite images, usually three methods are used: (a) terrain-dependent 3D rational functions without vendor image support data, (b) terrain-independent or refined 3D rational functions with vendor image support data, and, (c) 3D physical models.

Terrain-dependent 3D Rational Functions Without Vendor Image Support Data

The 3D rational function mathematical models built a correlation between the pixels (2D image space) and their ground locations (3D object space), as any other sensor model. This correlation is based on ratios of polynomials. For the ground-to-image transformation, the defined ratios of polynomials have the forward form:

$$x = \frac{P_1(X,Y,Z)}{P_2(X,Y,Z)} \qquad y = \frac{P_3(X,Y,Z)}{P_4(X,Y,Z)} \tag{1}$$

where x and y are the row and column in the image respectively, X, Y, and Z are the coordinates of points in object space, and, P_i (i = 1, 2, 3, and 4) are polynomial functions with the following general form:

$$\begin{aligned} Pi = {} & a_{1_i} + a_{2_i}X + a_{3_i}Y + a_{4_i}Z + a_{5_i}XY + a_{6_i}XZ + a_{7_i}YZ \\ & + a_{8_i}X^2 + a_{9_i}Y^2 + a_{10_i}Z^2 + a_{11_i}XYZ + a_{12_i}X^3 + a_{13_i}XY^2 \\ & + a_{14_i}XZ^2 + a_{15_i}X^2Y + a_{16_i}Y^3 + a_{17_i}YZ^2 + a_{18_i}X^2Z \\ & + a_{19_i}Y^2Z + a_{20_i}Z^3. \end{aligned} \tag{2}$$

Usually, rational functions are expressed by third order polynomials (Equation 1), though the number of coefficients in the polynomials can be reduced gradually.

There are several names used to refer these polynomial coefficients, such as rational function coefficients (RFCs), rational polynomial coefficients (RPCs), rapid positioning capability (RPC), and rational polynomial camera (RPC) data. The RPC often refers to rational functions with third order polynomials, while the rational function model (RFM) is used to general rational functions with some variations, as is the case with terrain-dependent rational functions.

In the terrain-dependent 3D rational functions without vendor metadata, the unknown polynomial coefficients must be computed for the user with GCPs collected in a conventional way (e.g., from maps, GPS, DGPS). Bearing in mind that the first coefficient in the denominator is usually known (a_1 = 1) a minimum of 7, 19, and 39 GCPs are required to resolve the first-, second-, and third-order rational polynomial function, respectively.

According to some researchers, this method is not stable enough in operational environments, unless a large number of densely distributed GCPs, about twice the number of unknowns, are available (Toutin, 2004a; Tao and Hu, 2001). The accuracy depends on the number, location, and accuracy of GCPs (Tao and Hu, 2002; Toutin and Cheng, 2002; Tao *et al.*, 2004).

Terrain-independent 3D Rational Functions with Vendor Image Support Data

With the physical sensor model available for commercial satellite data vendors, the rational polynomial coefficients (RPCs) can be solved using an object grid with its nodes coordinates determined using the physical sensor model (Tao and Hu, 2001). Usually, third-order RPCs for the forward form are distributed by image vendor in very high-resolution sensors, such as Ikonos or QuickBird.

This method can be applied without GCPs (because of that it is called terrain-independent), although the accuracy obtained is not very good. In QuickBird images, results published showed root mean square errors in one dimension ($RMSE_{1D}$) between 2.4 m and 13.8 m with this method (Cheng *et al.*, 2003a; Cheng *et al.*, 2003b). A very interesting possibility of this method is that users can update or improve the accuracy of the rational function model, refining the image vendor coefficients by a few GCPs. In very high-resolution satellite imagery, the RPCs may be refined directly or indirectly (Hu *et al.*, 2004). Direct refining methods update the original RPCs themselves (Hu and Tao, 2002), while the indirect refining introduces complementary transformation (usually polynomial) in image or object space, and they do not change the original RPCs. A number of publications have reported results using variations of the indirect approach (Di *et al.*, 2003; Fraser and Hanley, 2003; Grodecki and Dial, 2003; Noguchi *et al.*, 2004).

3D Physical Models

Physical models, also named rigorous, parametric, or deterministic, fully reflect the geometry of viewing. For this purpose, it is necessary to include in the model camera timing, alignment and focal plane layout information, and a full set of satellite attitude and ephemeris information. QuickBird basic imagery provides a complete set of image acquisition metadata. This method provides the most accurate and complete geolocation data (Robertson, 2003) and has a great robustness over the full image using only a few GCPs (Cheng *et al.*, 2003a).

Study Site and Data Set

Study Site

The study site is situated in the province of Almería at south east of Spain. Concretely at the region of Campo de Níjar, near of Cabo de Gata's Nature Reserve. The area has an elevation range of between 50 m to 850 m above mean sea level and can be considered slightly hilly. Figure 1 shows the DEM of the study area on the European Datum ED50 with the Hayford International Ellipsoid and projection UTM 30 N.

QuickBird Panchromatic Basic Imagery

DigitalGlobe's QuickBird satellite provides the largest swath width and highest resolution of any commercial satellite currently available. On 19 December 2004, a QuickBird panchromatic basic image was acquired. The basic scene was centered on the geographic coordinates WGS84 of

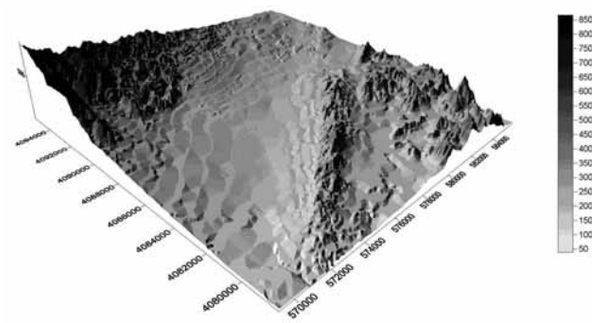

Figure 1. Digital elevation model of the study area on the European Datum ED50 with Hayford International Ellipsoid and projection UTM 30 N (orthometric elevations in meters).

36.93045°N and 2.12685°W. Other characteristics of the basic image are shown in Table 1.

Basic Imagery products are radiometrically corrected and sensor corrected, but not geometrically corrected or mapped to a cartographic projection and ellipsoid. Image resolution varies between 0.61 m (at nadir) to 0.72 m (25° off-nadir look angle) for panchromatic products. Basic imagery comes accompanied by Image Support Data (ISD) files including attitude and ephemeris data, geometric calibration, camera model, image metadata, radiometric data, and rational polynomial coefficients.

Ground Control Points Collection

A color photogrammetric flight at an approximate scale of 1:5000 with 60 percent and 30 percent longitudinal and transversal overlap, respectively, was commissioned by the Public Enterprise for Agriculture and Fishery of Andalusia (DAP) and carried out on 15 May 2001 covering a surface of around 160 km^2 in Almería, Spain. The photographs were scanned using a Vexcel UltraScan® 5000 photogrammetric scanner at a geometric resolution of 20 μm per pixel and a radiometric one of 24-bits (8-bits per chanel RGB). From this flight, we generated digital cartography at a scale of 1:1000 and a DEM with a grid spacing of 2 m using four digital photogrammetric workstations: two with SOCET SET® from Leica Geosystems and two with ImageStation SSK Z/I Imaging from Intergraph™. For the ground control of this flight, more than 300 points were collected using DGPS receivers in both static and real-time kinematic mode, and both with post-processing (Aguilar *et al.,* 2005a).

The selection of the GCPs and ICPs used in this study was based on well-defined and homogeneously distributed points on the QuickBird image. Because of that, a high percentage of the points measured in the ground control of the flight carried out in 2001 were rejected. Besides, there were areas in the scene in which we did not have any points.

In February 2005, a new topographic campaign took place to obtain coordinates of new points that were well-defined in the QuickBird scene. Thus, a good final distribution of the GCPs was ensured coverage over the full QuickBird image. On this occasion, a total station Trimble™ DGPS 5700 was used only in real-time kinematic and post-processing mode. The goal was to obtain a reliable measurement of GCPs and ICPs with accuracy better than a decimeter.

For the sensor orientation of the QuickBird basic imagery, 45 uniformly distributed GCPs were used. Thus, the QuickBird scene was divided into nine equal sub-areas, inside each of which five control points were placed (Figure 2). Seventy-nine ICPs were extracted to assess the errors in the processes of sensor orientation and orthorectification. They were not used in any correction process. These ICPs were inside the area of which digital cartography at a scale of 1:1000, and a dense digital elevation model was available (inside of white polyline in Figure 2). The ICPs have an elevation range of between 68 m to 247 m, with 171 m as mean value.

The coordinates of the 124 points (GCPs plus ICPs) collected were also referred to the ED 50 European Datum (Hayford International Ellipsoid), using the UTM projection. The vertical datum will take the geoid as reference surface, adopting as null orthometric height point the mean level in the calm sea of Alicante (Spain).

Digital Elevation Models

An original satellite image (un-rectified) does not show features in their correct locations. Orthorectification transforms a central projection of the original image into a parallel projection. Therefore, it is necessary to correct the displacements due to the tilt of the sensor and to the relief of the terrain. In the orthorectification of satellite images of very high-resolution, in which high geometric accuracies are required, the participation of a DEM can be very important. For the generation of panchromatic orthoimages of QuickBird, three DEMs were tested:

1. A coarse DEM with a grid spacing of 20 m created by the Environment Council of the Andalusia Government from the 1:50000 National Topographic Map which supports a contour interval of 20 m.
2. A medium DEM with a grid spacing of 5 m was derived by ourself from digitized contour lines with an interval of 10 m, extracted from the 1:10000 Andalusia Topographic Maps series. The vector file was imported to OrthoEngine® from PCI Geomatica, and finite difference algorithms were used to interpolate the DEM.
3. A dense DEM with a grid spacing of 2 m generated from a photogrammetric aerial flight at an approximate scale of 1:5000 using stereo image matching into a digital photogrammetric workstation. This DEM was available only in the zone where digital cartography was carried out in 2001 (Figure 2).

The statistics of the vertical residuals between the three DEM's elevations and surveyed elevations were computed over 50 points measured by DGPS, and placed on the natural terrain (Table 2). The DEMs were interpolated using Multiquadratic radial basis functions (Aguilar *et al.*, 2005b).

Orthorectification and Geometric Quality Assessment

The error of the orthoimage can be expressed as the sum of the error in the sensor orientation phase plus the error due to the DEM, assuming that both are independent. In this case

TABLE 1. CHARACTERISTICS OF THE QUICKBIRD BASIC IMAGERY ACQUIRED AT THE STUDY SITE (GSD-GROUND SAMPLE DISTANCE)

Product	Catalog Id	Acquisition Date	Off-Nadir (Degrees)	Cloud Cover (%)	Environmental Quality	Image (km)	GSD (m)
QuickBird Basic Imagery PAN	1010010003761A01	19-12-2004	8°	6	90	16.5 × 16.5	0.62 × 0.62

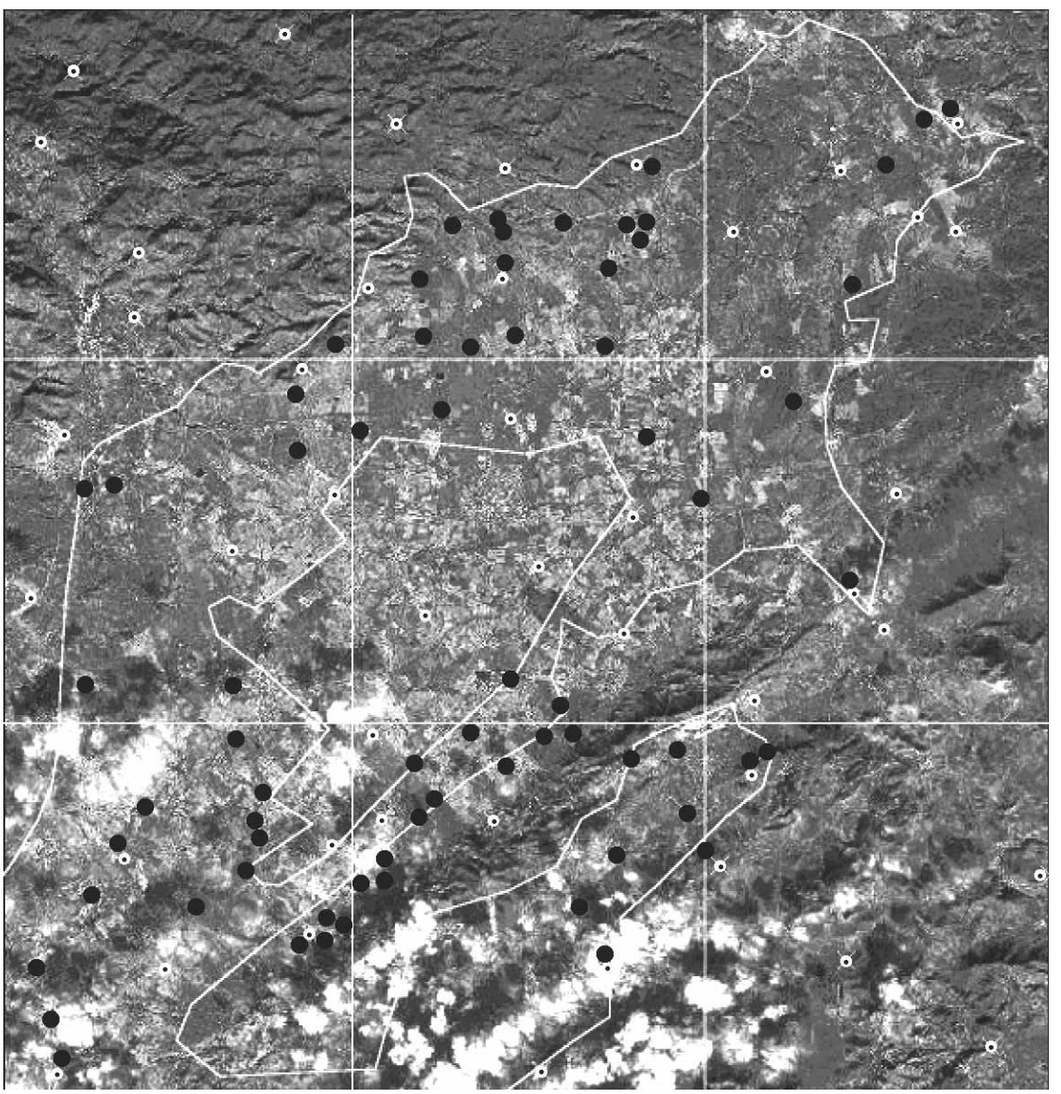

Figure 2. Distribution of ICPs (black circles) and GCPs (black points on white background) overlaid on the QuickBird Panchromatic Basic Imagery Orthorectified. The grid shows the division of the scene into equally sized areas to ensure a good distribution of GCPs chosen in every test. The white polyline encloses the area of which digital cartography at scale of 1:1000 and dense grid DEM were available.

TABLE 2. DESCRIPTIVE STATISTICS OF THE VERTICAL RESIDUALS FOR THE THREE DEMS USED

Grid Spacing (m)	Mean Error (m)	$RMSE_z$ (m)	Maximun Error (m)
2	0.13	0.31	0.65
5	−0.53	1.75	4.38
20	−1.71	5.82	−14.53

and applying the law of propagation of random errors, the following expression can be obtained:

$$\sigma^2_{ortho} = \sigma^2_o + \sigma^2_{DEM} \quad (3)$$

where σ_{ortho} is the standard deviation of the residuals in the orthoimage, σ_o is the standard deviation of the residuals after sensor orientation using the geometric correction model, and σ_{DEM} is the planimetric standard deviation related to the accuracy of the DEM. The standard deviation can be replaced by the RMSE when the mean of the residuals is zero, that is to say, there are not systematic errors.

Geometric Correction Models Tested

Four methods to calculate the sensor orientation are going to be tested in this work. All of them are supported by OrthoEngine® from PCI Geomatica which is the commercial software that we have used for the sensor orientation and orthorectification of the Campo de Níjar's QuickBird panchromatic basic scene.

Terrain-dependent 3D Rational Functions Without Vendor Image Support Data

First-order, terrain-dependent rational function model (RFM-1) is one of the models tested in this work. The election of first order polynomials instead of second- or third-order will be justified later. The RFM-1 model requires a minimum of seven GCPs for basic imagery.

Terrain-independent 3D Rational Functions with Vendor Image Support Data

In this work, PCI Geomatica OrthoEngine® software v.9.1 and update v. 9.1.7, developed by PCI Geomatics were used. The OrthoEngine® RPC indirect method is based on the block adjustment method developed by Grodecki and Dial (2003) for image space:

$$\begin{aligned} \Delta x &= x' - x = a_0 + a_1 x + a_2 y \\ \Delta y &= y' - y = b_0 + b_1 x + b_2 y \end{aligned} \tag{4}$$

where a_0, a_1, a_2, b_0, b_1, and b_2 are the adjustment parameters of an image, and Δx and Δy express the discrepancies between the measured line and sample coordinates for the new GCPs in the image space (x', y') and the RCPs projected coordinates for the same GCPs (x, y).

For Ikonos images, a zero order polynomial adjustment is adequate in most cases. In this case $\Delta x = a_0$ and $\Delta y = b_0$, where a_0 and b_0 are the bias parameters used by Fraser and Hanley (2003). At least one GCP is necessary to compute both parameters. The version 9.1 of PCI Geomatica OrthoEngine® only supports a zero order polynomial adjustment with vendor metadata (RPCV-0).

For QuickBird images, a first-order polynomial adjustment is required to achieve the best results. In this case, six coefficients have to be computed; therefore, it is necessary to know at least three GCPs. The version 9.1.7 of PCI Geomatica supports both zero (RPCV-0) and first order (RPCV-1) polynomial adjustment (Cheng *et al.*, 2005).

3D Physical Models

A 3D physical model developed by Dr. Toutin at the Canada Centre for Remote Sensing (CCRS) (Toutin and Cheng, 2002; Toutin, 2003) is tested in this work for the QuickBird basic imagery. This physical model, initially developed for medium-resolution sensors in the visible and infra-red as well as in the microwave (Toutin, 1995) was later adapted for QuickBird data (Toutin, 2004b). The CCRS model requires a theoretical minimum of six GCPs for basic imagery.

Design of Tests

In order to obtain the aims of the work, four tests carried out.

Geometric Accuracy Versus Number of GCPs, DEM, and Sensor Model

This test has been designed to study the influence of some variables on the geometric accuracy in the final orthoimage. These variables are the sensor model, the number of GCPs always well distributed in the scene and measured by DGPS, and the accuracy of the DEM used in the process of orthorectification.

Of the 45 measured GCPs using DGPS (Figure 2), combinations of n GCPs (n = 9, 18, 27, 36, and 45) were generated. The combination of nine GCPs was extracted choosing at random one GCP of the five located inside each of the sub-areas in which the QuickBird scene was divided (stratified random sampling). For the combination of 18 GCPs, two points per sector were chosen; for the one with 27 GCPs, three points per sector were chosen, and so on. The combinations of n GCPs remained constant in this test.

Five GCP combinations and four sensor orientation models were tested, thus, a total of 20 experimental data sets were generated. Once generated the 3D geometric correction models for every data sets, $RMSE_{1D}$, maximum errors and mean errors were computed in X and Y coordinates on 79 ICPs. Two dimensional root mean square errors ($RMSE_{2D}$) (Equation 5) were also calculated:

$$RMSE_{2D} = \sqrt{RMSE_x^2 + RMSE_y^2}. \tag{5}$$

Later on, the 20 sensor orientation data sets previously computed were used to generate orthorectified images. For this purpose, three DEMs (dense, medium, and coarse DEM) were used. $RMSE_{1D}$, $RMSE_{2D}$, maximum errors, and mean errors were computed again for the 79 ICPs on each one of the 60 orthorectified images generated.

The digital orthoimages created have a GSD of 0.6 m. In the process of orthorectification, the radiometric operation uses a resampling kernel applied to original image cells. The best results are obtained with the sinusoidal resampling kernel $(\sin(x)/x$ with 16×16 windows) (Toutin, 2004a) which was the resampling method used in the 60 orthorectified images generated in this work.

Determining the Best RFM Order

The same combinations of 9, 18, 27, 36, and 45 GCPs obtained previously were used to analyze the optimal number of polynomial coefficients computed for the terrain-dependent 3D rational functions without vendor image support data. The number of polynomial coefficients changed from 20 per polynomial (third-order rational function) to four per polynomial (first-order rational function). The $RMSE_{2D}$ in the sensor orientation phase was computed always in the same 79 ICP.

Reliability of the Accuracy Versus Distribution of GCPs and Sensor Model

When the number of GCPs used in the computation of the different sensor orientation models tested is small (9 or 18 GCPs), the variations in the results of the processes of orientation can be very dependent on the combination of chosen GCPs. In other words, the reliability of the determination of the unknown parameters of each mathematical approach becomes lower as was already noticed by Passini and Jacobsen (2004) in a scene of QuickBird. With GCPs measured by DGPS, the predominant error is generated by image pointing (Toutin and Chénier, 2004), and this error is different for every GCP. With this third test we try to calculate this degree of variation (confidence interval) of the accuracy for each of the sensor orientation models studied in this work. Besides, it is interesting to know as the distribution of the GCPs affects the geometric accuracy of the different models.

In this way, nine repetitions of 9 and 18 GCPs, respectively, were extracted from 45 initial GCPs. The samplings were carried out in two different ways: (a) completely random sampling (R), and (b) stratified random sampling (SR). Therefore, a total of 36 GCPs combinations were extracted. It seems to be clear that the distribution of 18 combinations of 9 and 18 GCPs carried out according to a completely random sampling is worse than those carried out by means of a stratified random sampling, due to the fact that in the first case, we can not ensure that at least one GCP per sub-area of QuickBird's scene is present in every extracted combinations.

The $RMSE_{2D}$ in the 79 ICPs was computed for every combination of GCPs. The variability of the $RMSE_{2D}$ around its mean value estimated for nine repetitions with regard to both types of samplings and the number of GCPs was represented as error bars at the 95 percent confidence interval.

Comparison Between Zero and First-order Polynomial Adjustments

Due to the fact that the terrain-independent rational functions can be calculated with few GCPs (or even without GCPs), the aim of this test was to compare the two terrain-independent 3D rational functions with vendor image support data, zero, and first-order polynomial adjustments, refined with nine or fewer GCPs. Four repetitions from one up to nine GCPs were extracted. The first one always belonged to the central sub-area of the QuickBird's scene and there were never two GCPs belonging to the same sub-area. In this test, again, the $RMSE_{2D}$ in 79 ICPs was used as an accuracy indicator in the sensor orientation phase.

Results and Discussion

Determining the Best RFM Order

Because it is difficult to determine which order of the RFM can provide the best result, and following the recommendations of Tao and Hu (2001), we decided to try different possibilities to determine the best RFM order for our data set.

Figure 3 shows the affect of the number of polynomial coefficients used in the rational function model for the terrain-dependent scenario and without vendor image support data on the geometric accuracy of the sensor orientation. The $RMSE_{2D}$ in the 79 ICPs follows a certain downward trend when the number of polynomial coefficients decreases. It is interesting to observe that when the number of GCPs used is near to the minimum needed to calculate a certain number of coefficients, the $RMSE_{2D}$ usually increase. For any number of GCPs, the $RMSE_{2D}$ at the ICPs presents the lowest values when we use only four coefficients per polynomial. Notice that only seven or more GCPs are necessary to calculate this solution. Because of this, the first order terrain-dependent rational functions (RFM-1) are studied in this work.

Geometric Accuracy Versus Number of GCPs, DEM, and Sensor Model

The errors generated in the sensor orientation phase in 79 ICPs and with five combinations of n GCPs are shown in Table 3. The RMSE in the ICPs reflect the restitution accuracy, which includes feature extraction error and are, therefore, a good estimation of the final positioning accuracy of planimetric features (Toutin and Chénier, 2004). The RMSE values are not affected, in general, by the number of well-defined and uniformly distributed GCPs that were used for the adjustment of the sensor orientation models. Only with RPCV-1 the RMSE seem to be slightly bigger when the number of GCPs is small (9 or 18). Something similar happened when RFM-1 was used with only nine GCPs. Besides, in these three cases and in all combinations of GCPs used with RPCV-0, inherent positional biases (mean errors greater than 0.15 m in absolute value) were detected on one of two axes (X or Y) that arise from systematic errors in the sensor orientation.

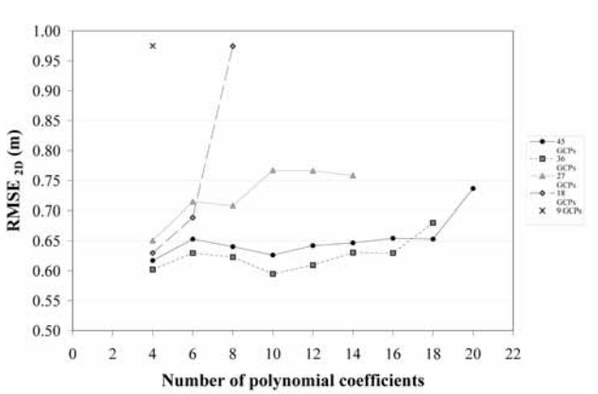

Figure 3. Effect of the number of polynomial coefficients used in the rational function model computed without image metadata on sensor orientation accuracy measured as two-dimensional RMSE at 79 ICPs for five combinations of GCPs.

The worst results of RMSE were generated when RPCV-0 was used ($RMSE_{2D}$ ranges between 1.29 m and 1.23 m), followed by RPCV-1 ($RMSE_{2D}$ ranges between 1.02 m and 0.82 m). RFM-1 and CCRS mathematical approaches produced the best results, if the combination of nine GCPs in RFM-1 is did not have into account. With these models $RMSE_{2D}$ around 0.63 m were obtained, which coincides with the GSD of our QuickBird basic image. The $RMSE_{2D}$ generated with RPCV-0 are approximately twice the GSD, while $RMSE_{2D}$ computed by RPCV-1 are approximately 1.36 $\times$ GSD.

On the other hand, the maximum errors of the residuals generated in the 79 ICPs are strongly linked to the corresponding $RMSE_{1D}$. In fact, the absolute value of maximum error produced in one dimension is very close to three times the value of the $RMSE_{1D}$.

In Figure 4, the relation between the two dimensional residuals obtained in each of 79 ICPs for the different combinations of n GCPs and the planimetric distance to the center of the image is presented. The 2D residuals increase linearly ($R^2 = 0.37$) with the distance to the center of the image when RPCV-0 is used (Figure 4a). This variation of the residuals obtained at the ICPs depending on the distance to the center of the image has not been generated by other sensor orientation models used. This again reflects the systematic errors generated by RPCV-0 mathematical approach.

The distribution of ground coordinate residuals in ICPs are represented in Figure 5 for the four sensor models tested and for 18 GCPs. Figure 5a shows residual systematic errors, principally in along-track direction, which are not being modeled by RPCV-0. This type of error distribution was already reported by Noguchi *et al.* (2004) and Fraser and Hanley (2005) for QuickBird stereo imagery. The along-track alignment of the vectors and their module are improved lightly when the RPCV-1 model is used (Figure 5b). Nevertheless, the best results are showed in the Figures 5c and 5d (RFM-1 and CCRS), where it is not possible to observe systematic errors in the represented vectors. This is very curious to observe, as the distribution of residuals in these models without vendor's rational polynomial coefficients is practically identical for any number of GCPs.

In previous research, when the CCRS model was used, $RMSE_{2D}$ values between 0.94 m and 1.13 m were reported in the sensor orientation phase on ICPs (Cheng *et al.*, 2003a; Cheng *et al.*, 2003b; Toutin and Chénier, 2004; Wolniewicz, 2004), although the GCPs used in some of this research work was less accurate than the GCPs used in our study. On the other hand, the number of ICPs used in these works was between 9 and 38, while that of GCPs changed between 6 and 10. For the RPCV-0 mathematical approach, $RMSE_{2D}$ between 1.44 m and 2.28 m were computed on ICPs (Cheng *et al.*, 2003a; Wolniewicz, 2004). In some research (Wolniewicz, 2004; Fiani *et al.*, 2004), the results relative to the sensor orientation by CCRS and RPCV-0 have been compared for the same QuickBird basic imagery and using PCI Geomatica. In these cases, the accuracies obtained using CCRS were better than the computed ones with RPCV-0. Niu *et al.* (2004) tested several adjustment models defined in image space in QuickBird stereo images and better results were obtained with RPCV-1 model than with RPCV-0.

TABLE 3. RMSE, MAXIMUM ERROR AND MEAN ERROR IN SENSOR ORIENTATION MEASURED IN 79 ICPS USING A DIFFERENT NUMBER OF GCPS AND FOUR 3D GEOMETRIC CORRECTION MODELS

		ICPs RMSE (m)			Maximum Error (m)		Mean Error (m)	
Model	GCPs	*X*	*Y*	2D	*X*	*Y*	*X*	*Y*
RPCV-0	9	0.65	1.11	1.29	−1.73	−3.37	−0.30	−0.48
	18	0.61	1.08	1.24	−1.63	−3.30	−0.20	−0.41
	27	0.58	1.09	1.23	1.76	−3.32	0.04	−0.43
	36	0.58	1.08	1.23	1.70	−3.29	−0.03	−0.40
	45	0.58	1.11	1.25	1.77	−3.36	0.04	−0.47
RPCV-1	9	0.69	0.74	1.02	−2.15	−1.67	−0.42	−0.19
	18	0.57	0.71	0.92	−1.87	1.89	−0.36	−0.02
	27	0.46	0.68	0.82	−1.60	1.77	−0.11	−0.04
	36	0.48	0.66	0.82	−1.55	1.75	−0.14	−0.04
	45	0.47	0.68	0.83	−1.45	1.77	−0.09	−0.06
RFM-1	9	0.43	0.87	0.97	−1.14	−3.23	0.15	−0.41
	18	0.46	0.43	0.63	1.15	−1.72	−0.02	−0.07
	27	0.45	0.46	0.64	1.26	−1.57	0.08	−0.07
	36	0.40	0.45	0.60	−1.20	−1.61	0.03	−0.05
	45	0.40	0.47	0.62	−1.21	−1.58	0.05	−0.05
CCRS	9	0.45	0.47	0.65	1.40	−1.49	0.10	−0.04
	18	0.42	0.46	0.62	−1.22	−1.59	−0.04	−0.09
	27	0.41	0.50	0.65	−1.10	−1.44	0.09	−0.13
	36	0.40	0.52	0.66	−1.17	−1.34	0.04	−0.11
	45	0.39	0.52	0.65	−1.19	1.35	0.06	−0.08

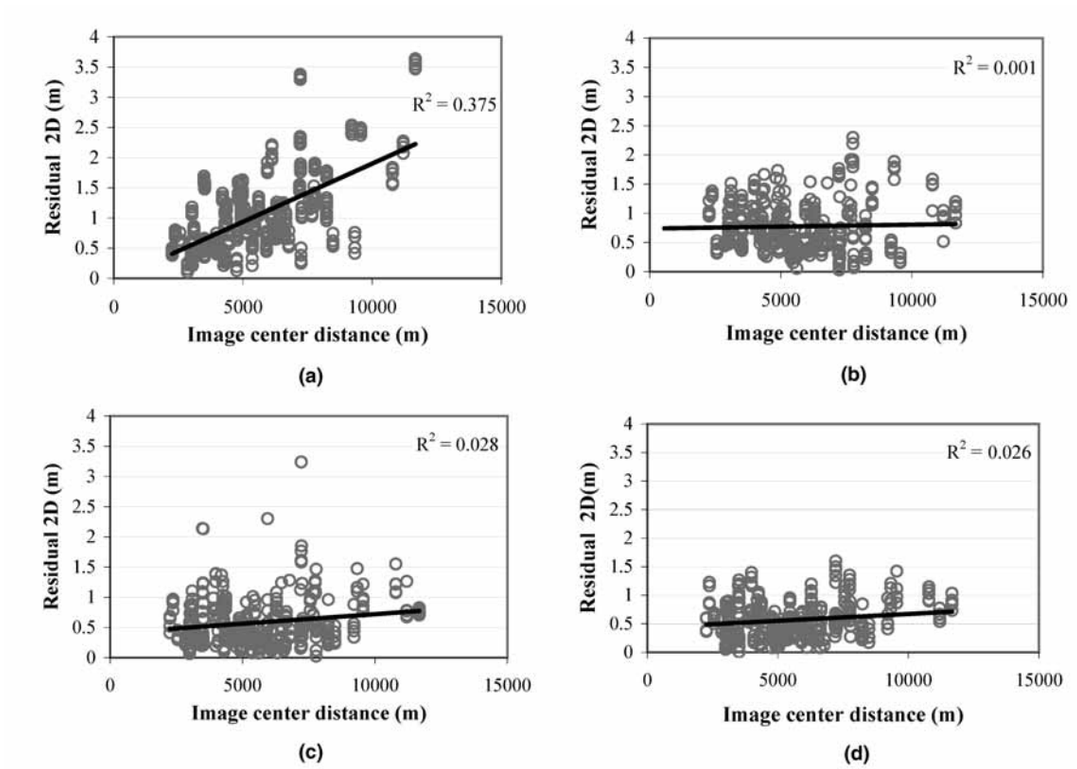

Figure 4. Variation of the two dimensional residuals in 79 ICPs depending on the distance to the center of the image for five combinations of GCPs: (a) Rational function with image metadata and zero order polynomial adjustment (RPCV-0), (b) Rational function with image metadata and first order polynomial adjustment (RPCV-1), (c) First-Order Rational function without image metadata (RFM-1), and (d) Physical model developed at the Canada Centre for Remote Sensing (CCRS).

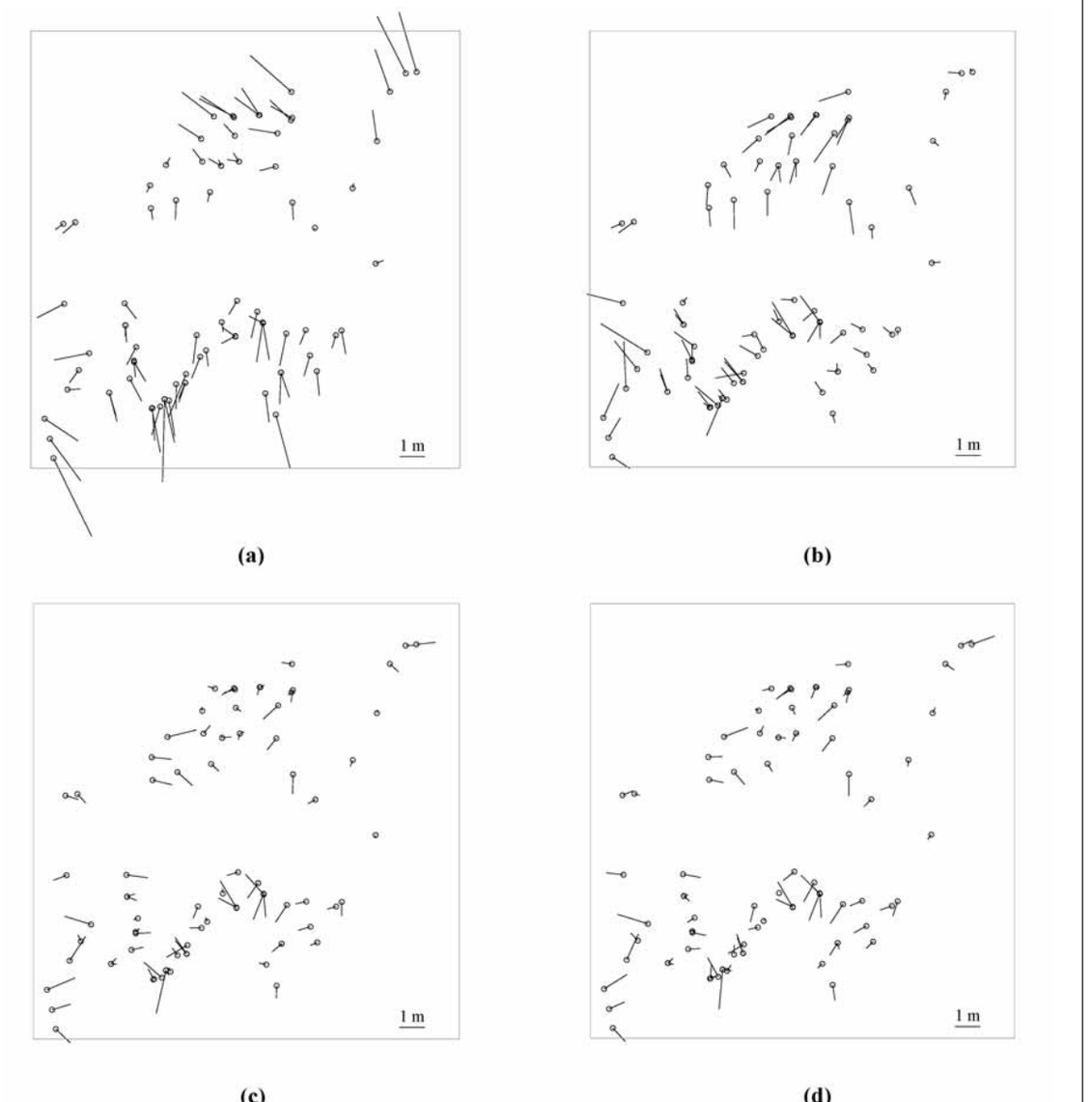

Figure 5. Ground coordinate residuals distribution in 79 ICPs for 18 GCPs: (a) Rational function with image metadata and zero order polynomial adjustment (RPCV-0), (b) Rational function with image metadata and first order polynomial adjustment (RPCV-1), (c) First-Order Rational function without image metadata (RFM-1), and (d) Physical model developed at the Canada Centre for Remote Sensing (CCRS)

Tables 4, 5, and 6 show the errors in 79 IPCs in the orthorectified images when the different DEMs are used. The results show trends very similar to those presented in the Table 3. This is logical if we bear in mind that the error produced in the orthoimage is the result of the sum of the error in the sensor orientation (Table 3) and that generated by the DEM (Equation 3). The possible systematic errors of the DEM can be reflected in the geometric accuracy of the orthoimage. This happened with the DEM with a spacing grid of 20 m, and it can be observed for all models in the mean errors presented in the Table 4.

The best geometric accuracy in the orthoimages was obtained when the dense DEM was used with CCRS or RFM-1 model (Table 6). In this case $RMSE_{1D}$ of between 0.45 m and 0.60 m were computed. When the medium DEM was used, slightly greater values of $RMSE_{1D}$ were computed (Table 5). Kay *et al.* (2003) reported $RMSE_{1D}$ on 28 ICPs in QuickBird basic orthorectified images around 1.15 m and a $RMSE_{2D}$ of 1.62 m when they used refined rational functions (RPCV-0) with only three or four GCPs and a DEM with $RMSE_z < 5$ m. The maximum $RMSE_{1D}$ recommended by the ASPRS interim accuracy standards (ASPRS, 1989) are 0.625 m, 1.25 m, and 2.50 m for 1:2500, 1:5000, and 1:10000 scale Class 1 product, respectively.

In Table 7, the $RMSE_{2D}$ related to the quality of the DEM (equivalent to σ_{DEM} in Equation 3) are showed for the three DEMs tested. In this study the residuals between the coordinates of each one of 79 ICPs after the sensor orientation, and

TABLE 4. RMSE, MAXIMUM ERROR AND MEAN ERROR IN 79 ICPS MEASURED IN THE ORTHORECTIFIED IMAGERY USING A COARSE DEM OF 20 M GRID SPACING ($RMSE_z$ = 5.82 M)

		ICPs RMSE (m)			Maximum Error (m)		Mean Error (m)	
Model	GCPs	*X*	*Y*	2D	*X*	*Y*	*X*	*Y*
RPCV-0	9	0.85	1.23	1.50	2.33	−4.08	−0.09	−0.69
	18	0.86	1.20	1.48	2.72	−3.84	0.01	−0.65
	27	0.87	1.18	1.47	2.64	−3.92	0.24	−0.64
	36	0.88	1.21	1.49	2.61	−4.11	0.19	−0.65
	45	0.88	1.23	1.51	2.69	−4.10	0.26	−0.70
RPCV-1	9	0.97	1.10	1.46	−2.88	−2.41	−0.23	−0.41
	18	0.91	1.04	1.38	−2.48	−2.35	−0.15	−0.24
	27	0.92	1.04	1.39	2.07	−2.42	0.10	−0.25
	36	0.92	1.02	1.37	2.27	−2.37	0.08	−0.28
	45	0.91	1.04	1.38	2.69	−2.18	0.19	−0.44
RFM-1	9	1.04	1.21	1.59	2.56	−4.00	0.33	−0.64
	18	0.87	0.80	1.18	2.34	−2.47	0.14	−0.32
	27	0.92	0.80	1.22	2.84	−2.24	0.28	−0.28
	36	0.89	0.79	1.19	2.55	−2.20	0.21	−0.26
	45	0.90	0.82	1.22	2.40	−2.23	0.22	−0.27
CCRS	9	1.03	0.79	1.30	2.28	−2.22	0.32	−0.31
	18	0.9	0.89	1.26	2.22	2.01	0.16	−0.22
	27	0.92	0.76	1.20	2.46	−1.97	0.33	−0.30
	36	0.9	0.74	1.17	2.29	−1.92	0.29	−0.34
	45	0.93	0.81	1.23	−2.32	−2.01	0.30	−0.37

TABLE 5. RMSE, MAXIMUM ERROR AND MEAN ERROR IN 79 ICPS MEASURED IN THE ORTHORECTIFIED IMAGERY USING A DEM OF 10 M GRID SPACING ($RMSE_z$ = 1.75 M)

		ICPs RMSE (m)			Maximum Error (m)		Mean Error (m)	
Model	GCPs	*X*	*Y*	2D	*X*	*Y*	*X*	*Y*
RPCV-0	9	0.82	1.26	1.50	−2.07	−3.44	−0.36	−0.55
	18	0.81	1.22	1.46	−2.05	−3.36	−0.29	−0.40
	27	0.78	1.24	1.46	−1.92	−3.44	−0.04	−0.47
	36	0.76	1.25	1.46	−1.97	−3.38	−0.07	−0.47
	45	0.76	1.28	1.49	−1.95	−3.49	0.01	−0.55
RPCV-1	9	0.82	0.77	1.13	−1.92	−1.90	−0.44	−0.25
	18	0.66	0.74	1.00	−1.63	−1.76	−0.38	−0.11
	27	0.56	0.73	0.92	−1.35	−1.82	−0.17	−0.16
	36	0.54	0.71	0.89	1.34	−1.86	−0.18	−0.14
	45	0.55	0.72	0.91	1.39	−1.84	−0.12	−0.12
RFM-1	9	0.50	0.89	1.02	1.14	−3.35	0.15	−0.47
	18	0.48	0.55	0.74	1.12	−2.03	−0.04	−0.14
	27	0.48	0.59	0.76	1.25	−1.87	0.06	−0.15
	36	0.51	0.58	0.77	1.41	−1.76	0.03	−0.10
	45	0.51	0.58	0.77	1.06	−1.75	0.06	−0.08
CCRS	9	0.49	0.61	0.78	1.41	−1.76	0.10	−0.12
	18	0.48	0.63	0.79	0.99	−1.93	−0.03	−0.17
	27	0.52	0.69	0.86	0.99	−1.64	0.10	−0.21
	36	0.52	0.68	0.86	1.28	1.58	0.03	−0.20
	45	0.50	0.65	0.82	−1.02	1.87	0.06	−0.14

the final coordinates after the orthorectification with a DEM were calculated. The $RMSE_{2D}$ generated by each of three tested DEMs did not depend of the sensor orientation models used. Values around of 0.47 m, 0.57 m, and 1.08 m were computed with dense, medium, and coarse DEMs, respectively. The importance of the quality of the ancillary data (DEM, GCPs) has again been confirmed in this study when very high-resolution sensors are used.

It must be emphasized that the possibility of having a dense DEM for image orthorectification is not very common. In this respect, the guidelines adopted by the European Commission for best practice in the orthorectification of very high-resolution imagery (European Commission, 2003), DEM with <5 m $RMSE_z$ height accuracy is required for off-nadir angles <15° and <2 m $RMSE_z$ for off-nadir angles >15°. In our case, with an off-nadir of 8°, the DEM with a grid spacing of 5 m is adapted to obtain good accuracy in the QuickBird's orthoimage.

The Andalusian government in Spain is very interested in creating and updating orthoimages across the whole area of Andalusia in order to use them for a variety of purposes (e.g., EU Common Agricultural Policy). In fact, it recently made a panchromatic orthophoto, based on a photogrammetric flight with an approximate scale of 1:20000 taken in 2001 and 2002, available for public viewing. The $RMSE_{1D}$ of this orthoimage were computed in 72 out of 79 ICPs used in this study, obtaining values of 0.95 m and 0.75 m for *X* and *Y*, respectively. Better $RMSE_{1D}$ results were obtained using the

TABLE 6. RMSE, MAXIMUM ERROR AND MEAN ERROR IN 79 ICPS MEASURED IN THE ORTHORECTIFIED IMAGERY USING A DEM OF 2 M GRID SPACING ($RMSE_z$ = 0.31 M)

		ICPs RMSE (m)			Maximum Error (m)		Mean Error (m)	
Model	GCPs	*X*	*Y*	2D	*X*	*Y*	*X*	*Y*
RPCV-0	9	0.78	1.12	1.36	−2.28	−3.64	−0.44	−0.42
	18	0.75	1.13	1.36	−2.10	−3.59	−0.34	−0.35
	27	0.66	1.10	1.28	−1.88	−3.65	−0.09	−0.38
	36	0.69	1.08	1.28	−1.94	−3.53	−0.17	−0.36
	45	0.67	1.10	1.29	−1.92	−3.69	−0.10	−0.41
RPCV-1	9	0.87	0.80	1.18	−2.11	−1.99	−0.58	−0.19
	18	0.70	0.79	1.06	−1.60	1.84	−0.52	0.02
	27	0.55	0.74	0.92	−1.39	−1.88	−0.26	−0.04
	36	0.56	0.72	0.92	−1.30	−2.04	−0.30	−0.04
	45	0.54	0.75	0.92	−1.28	−1.97	−0.24	−0.04
RFM-1	9	0.46	0.89	1.00	1.33	−3.68	0.02	−0.35
	18	0.52	0.51	0.73	−1.26	−2.06	−0.17	−0.03
	27	0.51	0.52	0.73	1.36	−2.01	−0.17	−0.04
	36	0.46	0.53	0.70	1.19	−1.92	−0.10	0.00
	45	0.47	0.55	0.72	−1.42	−2.05	−0.10	−0.03
CCRS	9	0.47	0.53	0.71	1.19	−1.82	−0.04	−0.01
	18	0.47	0.60	0.76	−1.18	−1.90	−0.16	−0.07
	27	0.45	0.59	0.74	1.17	−1.56	−0.03	−0.11
	36	0.47	0.57	0.74	−1.30	−1.56	−0.11	−0.11
	45	0.46	0.56	0.72	−1.23	1.52	−0.08	−0.07

TABLE 7. TWO DIMENSIONAL RMSE IN 79 ICPS RELATED TO THE QUALITY OF THE DEM

		DEM 2 × 2	DEM 5 × 5	DEM 20 × 20
Model	GCPs	$RMSE_{2D}$ (m)	$RMSE_{2D}$ (m)	$RMSE_{2D}$ (m)
RPCV-0	9	0.42	0.53	1.07
	18	0.45	0.58	1.06
	27	0.41	0.58	1.04
	36	0.43	0.59	1.05
	45	0.43	0.57	1.04
	Mean	**0.43**	**0.57**	**1.05**
RPCV-1	9	0.51	0.58	1.09
	18	0.51	0.69	1.09
	27	0.54	0.60	1.11
	36	0.51	0.56	1.11
	45	0.54	0.56	1.18
	Mean	**0.52**	**0.60**	**1.12**
RFM-1	9	0.49	0.57	1.16
	18	0.48	0.56	1.09
	27	0.56	0.56	1.06
	36	0.49	0.57	1.07
	45	0.48	0.58	1.08
	Mean	**0.50**	**0.57**	**1.09**
CCRS	9	0.43	0.56	1.07
	18	0.49	0.56	1.13
	27	0.42	0.57	1.04
	36	0.41	0.54	1.04
	45	0.41	0.56	1.06
	Mean	**0.43**	**0.56**	**1.07**

CCRS or RFM-1 models and a medium DEM ($RMSE_z$ = 1.75 m). Besides, we must bear in mind that the panchromatic image data of QuickBird has 11-bits (2,048 grey levels) instead of the classic 8-bits (256 grey levels). Thus, feature classification and identification can be notably improved.

Reliability of the Accuracy Versus Distribution of GCPs and Sensor Model

Figure 6 shows an analysis of the reliability, presented as confidence interval, of the geometric accuracy for each one of the four tested models when the number of GCPs is small (9 or 18). With only nine GCPs (Figure 6a), and extracted with a good distibution (SR), the best $RMSE_{2D}$ are generated by CCRS and RFM-1. In both models, the confidence intervals ranged between similar values, around 0.65 m and 1 m. In the Table 3, for nine GCPs, the values of $RMSE_{2D}$ computed for CCRS and RFM-1 models (0.65 m and 0.97 m, respectively) were inside the confidence interval, though coincidentally, they were on opposite ends of the range. The $RMSE_{2D}$ for RPCV-1 were lower than the computed ones for RPCV-0, and in both cases the confidence intervals were smaller than for CCRS and RFM-1. When nine GCPs were extracted according to a worse distribution (R), the results were deteriorated in all the sensor models, especially in RFM-1 and CCRS ones. In this case, there were no significant differences between sensor models (Figure 6a).

When 18 GCPs are used to compute the sensor models (Figure 6b), the affect of the type of sampling is significantly less important, because it is very difficult to extract a random combination of so many badly distributed points. In this case, again the best $RMSE_{2D}$ are computed by CCRS and RFM-1, although now, the confidence intervals are much smaller. They ranged between values of about 0.62 m and 0.76 m.

According to this, very good results can be calculated by only nine well-distributed GCPs in Quickbird's scene using CCRS or RFM-1. Nevertheless, to obtain a better reliability of the geometric accuracies is necessary to use 18 GCPs in the adjustment of these models.

Comparison Between Zero and First-order Polynomial Adjustments

If geometric accuracy is not the main objective or if the number of GCPs is highly restricted (less than nine), the use of sensor models based on the terrain-independent approaches (RPCV-0 and RPCV-1) would be justified. Figure 7 shows the $RMSE_{2D}$ computed by RPCV-0 and RPCV-1 using from one up to nine GCPs. With one and two GCPs only shift coefficients (a_0 and b_0 in the Equation 4) are computed in both models. When the number of GCPs changes from three up to seven, the RPCV-1 solutions are not numerically stable. Only from eight GCPs, the obtained results using RPCV-1 are clearly better that generated ones using RPCV-0.

One must consider that when using four GCPs or more, the mean $RMSE_{2D}$ of the four computed repititions in the 79 ICPs of either of the two sensor models have a value of less than 2.2 m.

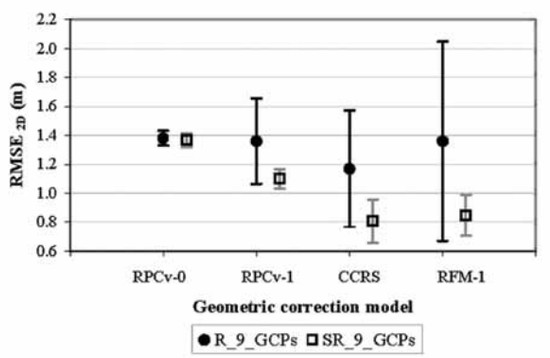

Figure 6. Two-dimensional RMSE in 79 ICPs with geometric correction model for two types of sampling, (R) Random sampling and (SR) Stratified random sampling. The black circles and the squares represents the mean values, and the error bars represent the 95 percent confidence interval for the estimation. (a) For nine repetitions of nine GCPs, and (b) For nine repetitions of 18 GCPs.

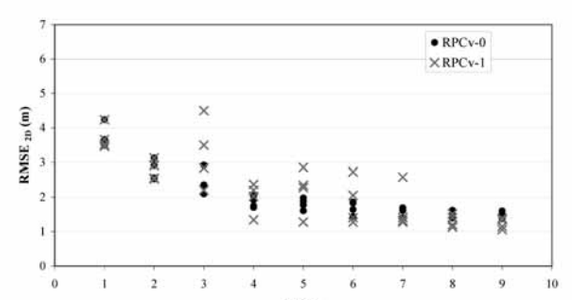

Figure 7. Variation of the two dimensional RMSE in 79 ICPs with the number of GCPs in the four repetitions for two rational function models computed with image metadata, zero (RPCV-0) and first order polynomial adjustments (RPCV-1). Notice that for one and two GCPs, the results are exactly equal because the mathematical models are the same.

However, the CCRS model can be calculated with only six GCPs and the RFM-1 with seven. In fact, these sensor models must also be taken into account in studies of six to eight GCPs.

Conclusions

Based on the numerous tests developed, the following conclusions can be drawn:

1. The best geometric accuracies obtained for a single QuickBird basic scene in the orientation phase of the sensor were found using the CCRS and the RFM-1. Using these two models and 18 or more well-distributed GCPs, the computed $RMSE_{2D}$ was approximately 0.63 m, while the $RMSE_{2D}$ of approximately 0.85 m and 1.24 m were generated using RPCV-1 and RPCV-0, respectively.

   Systematic biases were detected while using RPCV-0, and therefore, this mathematical approximation could only be applied to QuickBird basic images when the number available GCPs is very small (between one and five GCPS).
2. The reliablity of geometric accuracies obtained using CCRS and RFM-1 showed an important increase when 18 GCPs (extracted using random stratified sampling) were used instead of nine GCPs.

   With only nine GCPs extracted using random sampling, the results were worse across all models especially for the RFM-1. With the CCRS model, the confidence interval for the $RMSE_{2D}$ was almost three times greater than the one obtained when GCPs were extracted using stratified random sampling. Therefore, well-distributed GCPs are fundamental in order to obtain good and reliable, geometric accuracies using any sensor model especially when the number of GCPs used is not very high.
3. Errors in the orthoimage because of the relief are linked to the accuracy of the DEM used, although in our study, the sensor model and the number of GCPs used did not contribute to the errors that occurred.

   The best and most reliable results in the orthorectified images from a single QuickBird basic image in operational environment were obtained using the CCRS and RFM-1 models with no difference between them when 18 well-defined, uniformly-distributed (two in each cell of a 3×3 grid dividing the image) and accurate GCPS (DGPS measured) were used. Following this methodology $RMSE_{2D}$ about 0.74 m and 0.82 m were obtained using a dense DEM ($RMSE_z = 0.31$ m) and using a medium DEM ($RMSE_z = 1.75$ m), respectively.

The results obtained in this study using the RFM-1 model are very promising, since it is a simple mathematical approach that is supported by the majority of commercial satellite image processing packages. Nevertheless, it would be advisable to test this sensor model in QuickBird's new basic images changing the conditions of the relief, off-nadir or the quality of the GCPs.

Acknowledgments

The authors are grateful to the Public Enterprise for Agriculture and Fishery of Andalusia (DAP) for their collaboration in the preparation of this study. This research work has been financed by the project "Generation, integration and update of digital cartography as a support for rural sustainable development. Methodology and application in Campo de Níjar (Almería)" subsidized by the Andalusia Government.

References

Aguilar, M.A., F.J. Aguilar, J.A. Sánchez, F. Carvajal, and F. Agüera, 2005a. Geometric correction of the quickbird high resolution panchromatic images, *Proceedings of the XXII International Cartographic Conference*, 09–16 July, A Coruña, Spain, unpaginated CD-ROM.

Aguilar, F.J., F. Agüera, M.A. Aguilar, and F. Carvajal, 2005b. Effects of terrain morphology, sampling density, and interpolation methods on grid DEM Accuracy, *Photogrammetric Engineering & Remote Sensing*, 71(7):805–816.

ASPRS, 1989. ASPRS interim accuracy standards for large scale maps, *Photogrammetric Engineering & Remote Sensing*, 56(11):1038–1040.

Cheng, P., T. Toutin, and Y. Zhang, 2003a. QuickBird- Geometric correction, data fusion, and automatic DEM extraction, *Proceedings of the 24th Asian Conference on Remote Sensing (ACRS 2003) and 2003 International Symposium on Remote Sensing*, 03–07 November, Busan, Korea, unpaginated CD-ROM.

Cheng, P., T. Toutin, Y. Zhang, and M. Wood, 2003b. QuickBird-Geometric correction, path and block processing and data fusion, *Earth Observation Magazine*, 12(3):24–30.

Cheng, P., D. Smith, and S. Sutton, 2005. Mapping of QuickBird images using the RPC method improvement in accuracy since release of first QuickBird data, *GEOInformatics*, 8(4):50–52.

Chmiel, J., S. Kay, and P. Spruyt, 2004. Orthorectification and geometric quality assessment of very high spatial resolution satellite imagery for Common Agricultural Policy purposes, *Proceedings of the XXth International Archives of the Photogrammetry, Remote Sensing and Spatial Information Sciences*, 35(Part B4), 12–23 July, Istanbul, Turkey, unpaginated CD-ROM.

Di, K., R. Ma, and R. Li, 2003. Geometric processing of Ikonos Geo stereo imagery for coastal mapping applications, *Photogrammetric Engineering & Remote Sensing*, 69(8):873–879.

European Commission, 2003. Guidelines for Quality Checking of Ortho Imagery, URL: http://mars.jrc.it/marspac/CwRS/default.htm (last date accesed: 31 July 2007).

Fiani, M., P. Pistillo, S. Troisi, and L. Turturici, 2004. The role of ephemerides and GCPs distribution in high resolution satellite images modelling, *Proceedings of the XXth International Archives of the Photogrammetry, Remote Sensing and Spatial Information Sciences*, 35(Part B7), 12–23 July, Istanbul, Turkey, unpaginated CD-ROM.

Fraser, C.S., 2002. Prospect for mapping from high-resolution satellite imagery, *The 23rd Asian Conference on Remote Sensing (ACRS 2002)*, 25–29 November, Kathmandu, Nepal, unpaginated CD-ROM.

Fraser, C.S., H.B. Hanley, and T. Yamakewa, 2002. Three-dimensional geopositioning accuracy of Ikonos imagery, *The Photogrammetric Record*, 17(99):465–479.

Fraser, C.S., and H.B. Hanley, 2003. Bias compensation in rational function for Ikonos satellite imagery, *Photogrammetric Engineering & Remote Sensing*, 69(1):53–57.

Fraser, C.S., and T. Yamakewa, 2004. Insights into affine model for high-resolution satellite sensor orientation, *ISPRS Journal of Photogrammetry and Remote Sensing*, 58(2004):275–288.

Fraser, C.S., and H.B. Hanley, 2005. Bias-compensated RPCs for sensor orientation of high-resolution satellite imagery, *Photogrammetric Engineering & Remote Sensing*, 71(8):909–915.

Grodecki, J., and G. Dial, 2003. Block adjustment of high-resolution satellite images described by rational polynomials, *Photogrammetric Engineering & Remote Sensing*, 69(1):59–68.

Hu, Y., and C.V. Tao, 2002. Updating solution of the rational function model using additional control information, *Photogrammetric Engineering & Remote Sensing*, 68(7):715–724.

Hu, Y., C.V. Tao, and A. Croitoru, 2004. Understanding the rational function model: Methods and applications, *Proceeding of the XXth* International Archives of the Photogrammetry, Remote Sensing and Spatial Information Sciences, 35(Part B5), 12–23 July, Istanbul, Turkey, unpaginated CD-ROM.

Jacobsen, K., 2002. Generation of orthophotos with Carterra Geo images without orientation information, *Proceedings of the ACSM-ASPRS Annual Conference/XXII FIG International Congress*, 19–26 April, Washington D.C., unpaginated CD-ROM.

Kay, S., P. Spruyt, and K. Alexandrou, 2003. Geometric quality assessment of orthorectified VHR space image data, *Photogrammetric Engineering & Remote Sensing*, 69(5):484–491.

Lingua, A., and E. Borgogno, 2003. High resolution satellite images orthoprojection using dense DEM, *Proceedings of SPIE, Image and Signal Processing for Remote Sensing VIII*, 4885:433–443.

Niu, X., J. Wang, K, Di, J. Lee, and R. Li, 2004. Geometric modelling and photogrammetric processing of high-resolution satellite imagery, *Proceeding of the XXth International Archives of the Photogrammetry, Remote Sensing and Spatial Information Sciences*, 35(Part B4), 12–23 July, Istanbul, Turkey, unpaginated CD-ROM.

Noguchi, M., C.S. Fraser, T. Nakamura, T. Shimono, and S. Oki, 2004. Accuracy assesment of QuickBird stereo imagery, *The Photogrammetric Record*, 19(106):128–137.

Passini, R., and K. Jacobsen, 2004. Accuracy analysis of digital orthophotos from very high-resolution imagery, *Proceeding of the XXth International Archives of the Photogrammetry, Remote Sensing and Spatial Information Sciences*, 35(Part B4), 12–23 July, Istanbul, Turkey, unpaginated CD-ROM.

Pecci, J., F. Cano, and G. Maza, 2004. Generación de una ortoimagen QuickBird del año 2003 de la comunidad autónoma de la región de Murcia: Metodología y resultados, *XI Congreso Métodos Cuantitativos, Sistemas de Información Geográfica y Teledetección*, 20–23 September, Murcia, Spain, pp. 301–312.

Robertson, B.C., 2003. Rigorous geometric modelling and correction of QuickBird Imagery, *Proceedings of International Geoscience and Remote Sensing Symposium (IGARSS)*, 21–25 July, Toulouse, France, pp. 797–802.

Rossi, L., and F. Volpe, 2005. Integrated cadastre system for EU agricultural subsidies. Italian response to the challenge of environmental sustainability, *GEOInformatics*, 8(4):12–13.

Tao, C.V., and Y. Hu, 2001. A comprehesive study of the rational function model for photogrammetric processing, *Photogrammetric Engineering & Remote Sensing*, 67(12):1347–1357.

Tao, C.V., and Y. Hu, 2002. 3-D reconstruction methods based on the rational function model, *Photogrammetric Engineering & Remote Sensing*, 68(7):705–714.

Tao, C.V., Y. Hu, and W. Jiang, 2004. Photogrammetric exploitation of IKONOS imagery for mapping applications, *International Journal of Remote Sensing*, 25(14):2833–2853.

Toutin, T., 1995. Multi-source data integration with an integrated and unified geometric modelling, *EARSeL Journal Advances in Remote Sensing*, 4(2):118–129.

Toutin, T., and P. Cheng, 2002. QuickBird- A milestone for high-resolution mapping, *Earth Observation Magazine*, 11(4):14–18.

Toutin, T., 2003. Error tracking in Ikonos geometric processing using a 3D parametric model, *Photogrammetric Engineering & Remote Sensing*, 69(1):43–51.

Toutin, T., 2004a. Geometric processing of remote sensing images: Models, algorithms and methods, *International Journal of Remote Sensing*, Review Article, 25(10):1893–1924.

Toutin, T., 2004b. Comparison of stereo-extracted DTM from different high-resolution sensors: SPOT-5, EROS-A, IKONOS-II, and QuickBird, *IEEE Transactions on Geoscience and Remote Sensing*, 42(10):2121–2129.

Toutin, T., and R. Chénier, 2004. CGP requeriment for high-resolution satellite mapping, *Proceedings of the XXth International Archives of the Photogrammetry, Remote Sensing and Spatial Information Sciences*, 35(Part B3), 12–23 July, Istanbul, Turkey, unpaginated CD-ROM.

Wong, K.W., 1980. Basics mathematics of photogrammetry, *Manual of Photogrammetry*, Fourth edition (C.C. Slama, editor), American Society of Photogrammetry, Falls Church, Virginia, pp. 37–101.

Wolniewicz, W., 2004. Assessment geometric accuracy of VHR satellite images, *Proceedings of the XXth International Archives of the Photogrammetry, Remote Sensing and Spatial Information Sciences*, 35(Part B1), 12–23 July, Istanbul, Turkey, unpaginated CD-ROM.

Zhou, G., and R. Li, 2000. Accuracy evaluation of ground points from Ikonos high-resolution satellite imagery, *Photogrammetric Engineering & Remote Sensing*, 66(9):1103–1112.

(Received 17 March 2006; accepted 31 March 2006; revised 18 April 2006)